ECE 445

SENIOR DESIGN LABORATORY

FINAL REPORT

High efficient resonance tank design and output voltage control for wireless power transfer system

---

Team #39

WANG YUHANG

(yuhang.21@intl.zju.edu.cn)

JING LIHENG

(liheng.21@intl.zju.edu.cn)

WEI YUHANG

(yuyang.21@intl.zju.edu.cn)

DONG HONGYE

(hongye.21@intl.zju.edu.cn)

TA: Sheng Jing

May 17, 2025

Abstract

In this report, the design of a self-navigating, wirelessly charged car is presented. The report includes the problem addressed by the design, how the project is conducted, and future possibilities. There are generally four main parts of work: RaspberryPi for mapping, STM32 micro-controller for motor controlling, wireless charging coils and compensating circuit, and the mechanical hanger of coils and basement. There are concessions made and justified. The design of each part is also simulated and integrated into experimental environment.

Contents

1 Introduction

1.1 Purpose

In light of national carbon peaking and carbon neutrality goals, along with the rapid development of artificial intelligence, smart electric vehicles as a backbone force in reducing carbon emission and air pollution mitigation showcasing its potential to become a vital component of future vehicle industry. However, one of the largest obstacles in the promotion of electric vehicles (EVs)is the capacity of batteries. Wireless charging, also known as wireless power transfer (WPT), is the technology that enables a power source to transmit power through an air gap to electrical devices for the purpose of energy replenishment. [1] However, due to low mutual induction between the transmitter and receiver coils and low transmission factor, efficiency in WPT has long been a problem we have to live with. [2] Another problem with WPT technologies is the time slot where charging should be stopped for prolonging the lifetime for components and energy saving.

In order to mitigate the effects of the aforementioned problems, we propose a prototype of wireless charging systems for electric vehicles including a car and a charging station. The car will have hill-climbing algorithm for a Maximum Power Point Tracking(MPPT). The circuits of transmitter and receiver sides will be designed such that resonance and efficiency are obtained at the same time. We also propose an integrated station which will ensure a stable condition for such hill-climbing process.

1.2 Functionality

A 12V battery is used as the energy storage. The car can move at a maximum speed of 1 m/s. The wireless charging can give the battery's rated charging voltage. The car can align to the charging coil within 7 minutes automatically. The place of the charging station is recognized by a special obstacle on the map. Three boxes are avoided during the navigation process.

Together, the high-level requirements mentioned above will integrate into a self-navigating car which can be charged wirelessly. The outcome of the entire system meets the overall

purpose which is to build an automatic wireless charging car.

1.3 Subsystem Overview

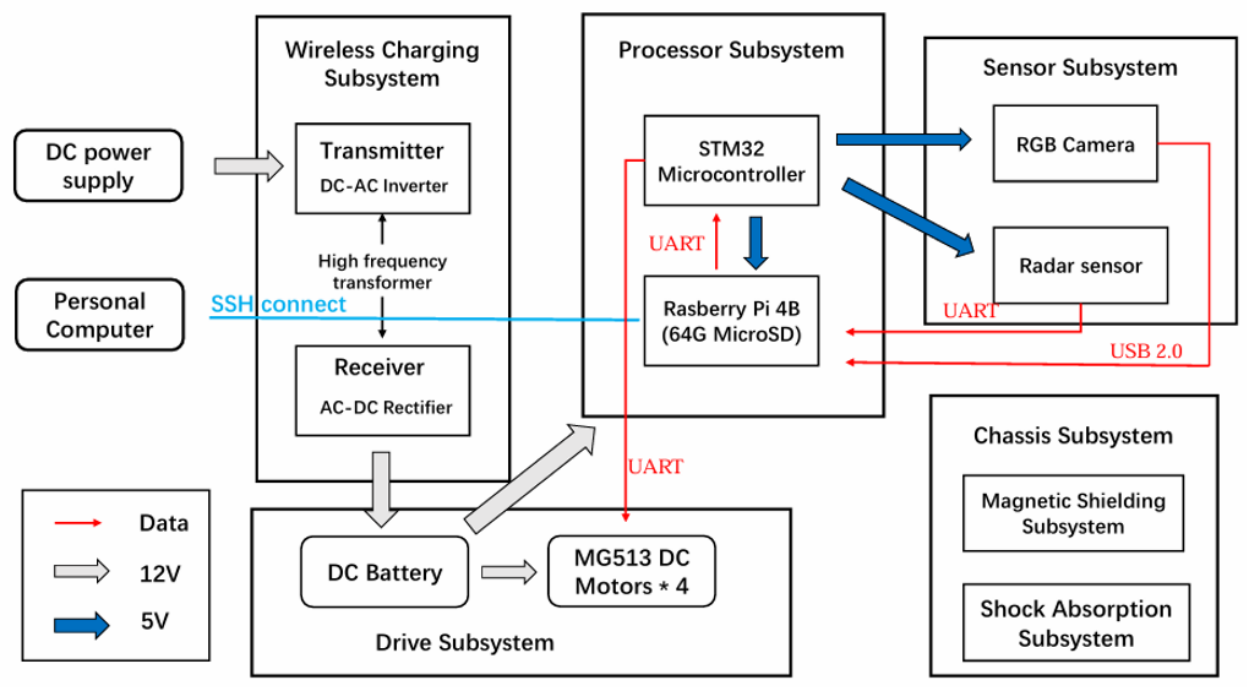

Figure 1: Project Overview

Our autonomous ROS-based vehicle system integrates five key subsystems that work synergistically to enable intelligent operation. The Wireless Charging Subsystem, comprising a DC-AC inverter transmitter with high-frequency transformer and an AC-DC rectifier receiver, provides continuous power without physical connections. At the core lies the Processor Subsystem, where a Raspberry Pi 4B (64GB MicroSD) running Ubuntu serves as the central brain, hosting navigation algorithms and communicating via UART with an STM32 microcontroller. Environmental perception is handled by the Sensor Subsystem's RGB camera and radar sensor, which feed data to the Raspberry Pi through UART and USB 2.0 interfaces. The Raspberry Pi processes this sensory data, generates ROS velocity control nodes that are subscribed by the STM32, which then converts these commands into signals for the Drive Subsystem's four MG513 DC motors. All components are mounted on a robust Chassis Subsystem featuring magnetic shielding for elec-

tromagnetic isolation and shock absorption for mechanical stability. The entire system can be remotely controlled via SSH connection from a host PC running Ubuntu, creating a seamless pipeline from sensor input to motor output while maintaining continuous wireless power delivery.

2 Design

2.1 Equations & Simulations

The main topology that will be discussed in this article is a bidirectional CLLC converter which has drawn much attention for symmetrical structure, ZVS region. As shown in Figure, a CLLC converter is composed of symmetrical full-bridge switches on primary and secondary sides, LC resonant circuit on both sides, and input output terminals. One note about this diagram is that we have considered leakage inductances on primary and secondary sides included in L1 and L2. The circuit topology without control signals are shown in fig.2 in the actual circuit we can practically plug in the impedances and get the

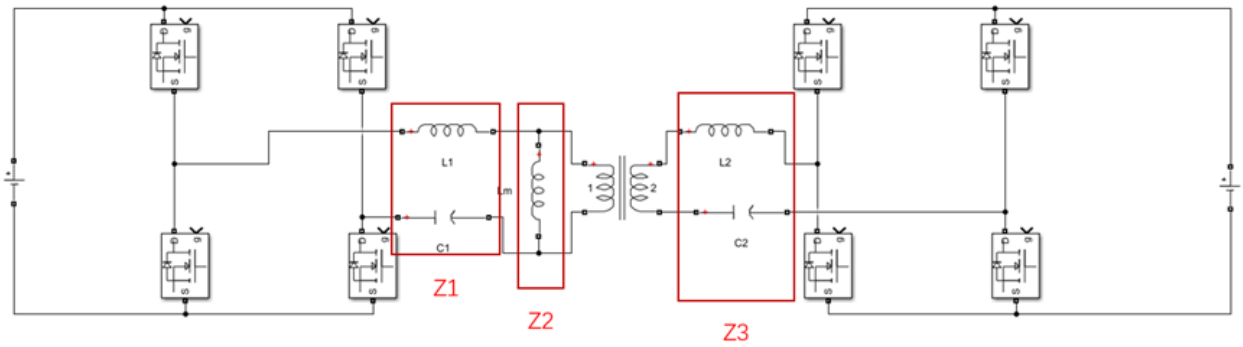

Figure 2: Circuit Topology of Bidirectional CLLC Circuit

following condition as in equation1 and achieve a constant output voltage as shown in equation2.

$$\begin{aligned}\left(j\omega L_1+\frac{1}{j\omega C_1}\right)\left(j\omega L_2+\frac{1}{j\omega C_2}\right)\\ +\left(j\omega L_1+\frac{1}{j\omega C_1}\right)(j\omega L_m)\\ +\left(j\omega L_2+\frac{1}{j\omega C_2}\right)(j\omega L_m)=0\end{aligned} \tag{1}$$

$$\text{Gain}=\left|\frac{Z_3}{Z_1+Z_3}\right| \tag{2}$$

However, there are 6 parameters needed for satisfaction of equation 1, including frequency of fundamental harmonic. Some of the parameters' adjustments also need to

consider practical limits, such as L1 and L2. An easy way to overcome this is to eliminate Z1 and Z2 by making their resonant frequency equal to switching frequency. Another rule we need to consider is gain function. As in practice Z3 is determined by the coils, We need to make sure that Z1 is tuned as needed to control gain.

To verify the wireless charging system and to instruct the input and output ratings of the vehicle, a Simulink model is built as shown in fig.2. Its ZVS and ZCS functions are verified. And the voltage and current around the wireless coils are analyzed in this chapter. The life of MOSFET components are be porlonged if they are working in ZVS zone of the circuit.

To analyze different phase of either resonance or linear charging of the inductor, I will focus on the analysis of voltage. From top to bottom, there are waveforms of four voltages which are separately: voltage going out of the full bridge (square wave), voltage of magnetizing inductance of the coils, voltage of transmitter resonance branch, and voltage across receiver resonance branch. The meaning of resonance branch is the combination of capacitor and inductor on either side. The charging and discharging of magnetizing inductor results in a linear voltage which is clamped by the resonant voltage when it is smaller than the resonant voltage. This will be seen at the transition between linear and sinusoidal wave at the forward or reversed voltage intervals of input square wave.

To analyze different phase of either resonance or linear charging of the inductor, I will focus on the analysis of voltage. As shown in fig.3, from top to bottom, there are waveforms of four voltages which are separately: voltage going out of the full bridge (square wave), voltage of magnetizing inductance of the coils, voltage of transmitter resonance branch, and voltage across receiver resonance branch. The meaning of resonance branch is the combination of capacitor and inductor on either side. The charging and discharging of magnetizing inductor results in a linear voltage which is clamped by the resonant voltage when it is smaller than the resonant voltage. This will be seen at the transition between linear and sinusoidal wave at the forward or reversed voltage intervals of input square wave.

As for transmitter and receiver resonance branch, they have the same shape with near-

sinusoidal wave deviating for the linear charging process. If we look at the waves closely, it can be found that the switching frequency is low so that we have passed half of the resonant wave. The outputs will also be clamped by the linear wave if we lower the switching frequency to cross the threshold.

For the driving part of the circuit, I used a waveform generator which can support a square wave up to 100 kHz. According to the previous analysis and the result we got from browsing commercially used frequencies for wireless charging, we decided on a 85 kHz drive signal. By looking at the datasheet of the MOSFETs used, the drive signal should have a lower edge at 0V and an upper edge at 4 V. In summary, the drive signal is a square wave with 4 V Vpp and a frequency of 85 kHz.

In conclusion, at a frequency of 85kHz, we have a combination of different working modes. However, the linear region takes only a small portion in the near-zero region of the sinusoidal wave, leaving a minor effect. Thus, we expect a good current output from the receiver side.

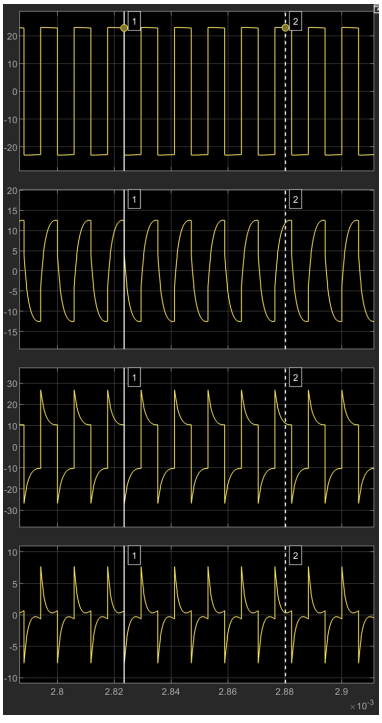

Figure 3: The Voltage Waveform of the Charging Coils

2.2 Design Alternatives

The charging power is not reached as pre-assumed 20W because the maximum charging voltage for the battery is 12.6V. Even if we could reach higher charging voltage and higher charging power, it may damage the battery or even cause safety issues. So we are settled at making sure the 12.6V charging voltage is reached.

The RaspberryPi lost its SSH connection near the final demo. We debugged for hours and found that it was burnt when we were trying to connect the power supervisor module(INA219).

There was a collision of interests between making it easier for the vehicle to move onto the basement smoothly and making the reciever coil as low as possible for better coupling. By manual adjustments and trials, we found the boundary height where the car can move onto the base.

There are multiple modules wired together using DuPont wire. Long wires were dragged on the ground or stuck in wheels. We solved this by using straps and tapes to fix the loose wires onto the car.

2.3 Design Description & Justification

2.3.1 Wireless Charging System

In our practical application, we will use PCB boards to simulate real wireless power transfer. Two PCB boards will be applied to form a CLLC charging system, with the capacitor and inductor values adjusted to meet charging requirements. The choice of such topology is verified by simulation and derivation described in section 2.1. The schematics are shown in section 2.4.

To meet the project's requirements, we use multi-strand enamel-insulated wire for the excitation coil with a sufficiently large cross-sectional area. Multi-strand enamel-insulated wire for excitation coils typically refers to a type of conductor used in exciting electromagnetic devices. It consists of multiple strands of insulated wire or bare copper wire, often

coated or wrapped in insulating material to enhance electrical insulation performance. The main feature of this wire is its large surface area, which disperses alternating current, thereby mitigating the skin effect. The coils are circular with 7.5 centimeters in radius. In experiment, we figured that a larger area of the coils not only eases the alignment process, but also gives a larger efficiency of voltage transmission. However, the area of the reciever coil is limited by the width of the car. The reciever coil is required to be within the width of the car because it needs to be clipped under the car.

2.3.2 Chassis Subsystem

In the shock absorption subsystem, we have designed four independent hydraulic spring shock absorbers. Each wheel has an independent shock absorption system, which can effectively ensure the level of the entire car chassis, thereby ensuring that the charging coil on the car can be parallel to the charging coil of the charging base station, further improving the efficiency of wireless charging. When installing, first install two acrylic shock absorber plates 1 (as shown in Figure 5) and two acrylic shock absorber plates 2 (as shown in Figure 6) on the metal frame (as shown in Figure 4) to connect the hydraulic spring shock absorber to the metal frame and limit the working space of the shock absorber. In the design, hydraulic spring shock absorbers are installed between two flat plates and a base plate (as shown in Figure 8). When the wheels are driving on uneven roads, the shock absorbers are compressed by the terrain and the weight of the car itself to maintain the balance of the car chassis. At the same time, when encountering large impacts, the shock absorbers can absorb the impact from the road surface, reduce the damage caused by the impact through repeated vibrations, and enable the car to recover to normal driving status faster, providing better stability and durability for the car.

2.3.3 Sensor Subsystem

The Sensor Subsystem serves as the vehicle's perception module, enabling environmental awareness and autonomous navigation capabilities. At its core, the system integrates a Leishen N10P LiDAR sensor and an ASTRA S RGBD camera to provide complementary

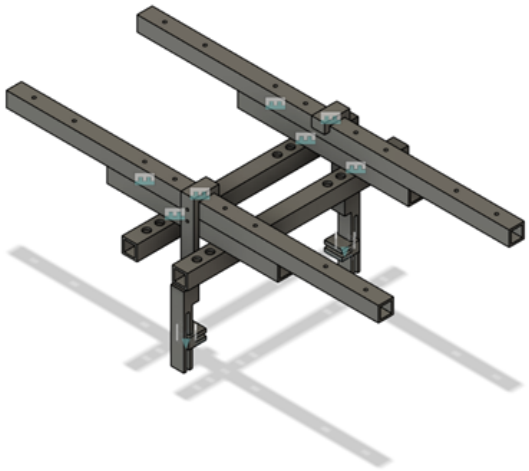

Figure 4: Metal Frame

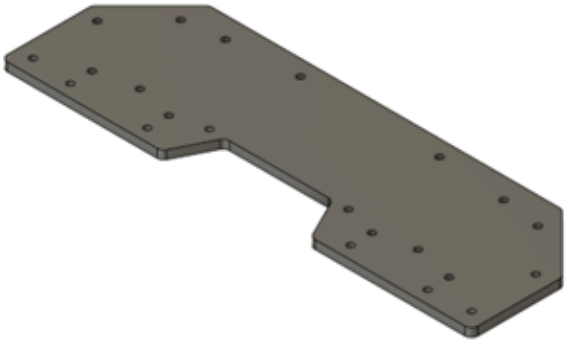

Figure 5: Acrylic Shock Absorber Plates 1

d

sensing modalities. The LiDAR delivers high-precision 2D point cloud data for spatial mapping, while the RGBD camera contributes visual texture information and depth perception, enhancing the system's ability to interpret complex environments. For mapping and localization, we employ the gmapping algorithm, a widely adopted open-source solution based on a particle filter SLAM (Simultaneous Localization and Mapping) framework. Gmapping utilizes Rao-Blackwellized particle filters to simultaneously estimate the robot's pose and construct an occupancy grid map of the environment. Each particle in the filter represents a potential trajectory hypothesis, with associated map updates

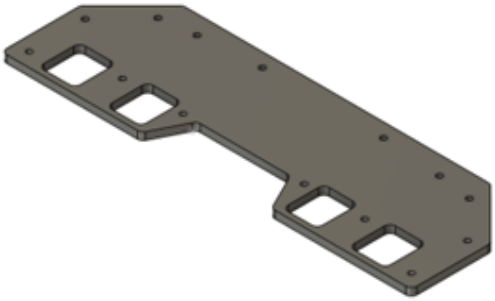

Figure 6: Acrylic Shock Absorber Plates 1

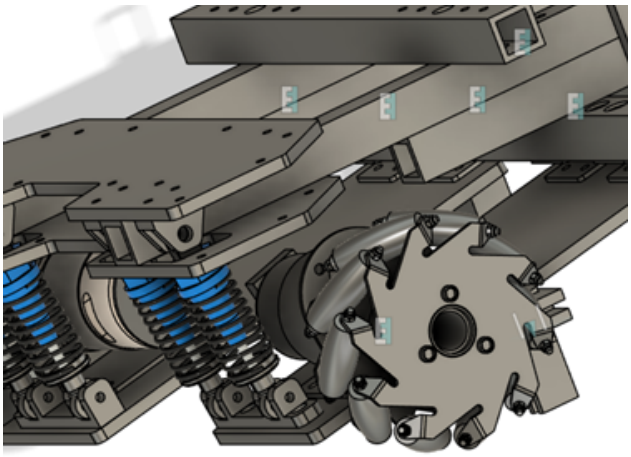

Figure 7: Shock Absorption Subsystem

weighted by sensor data consistency. This approach efficiently balances computational load with mapping accuracy, making it ideal for real-time operation on our Raspberry Pi platform. The mapping process begins with manual teleoperation of the vehicle through the target environment. During this phase, the LiDAR continuously scans surroundings while odometry data tracks movement. Gmapping processes these inputs to incrementally build a detailed occupancy grid, visualized in RViz, as shown in Figure 7. Completed maps can be saved for future reuse. Autonomous navigation leverages the generated map through a costmap-based planning stack. In RViz, users simply click-and-drag to set navigation targets.

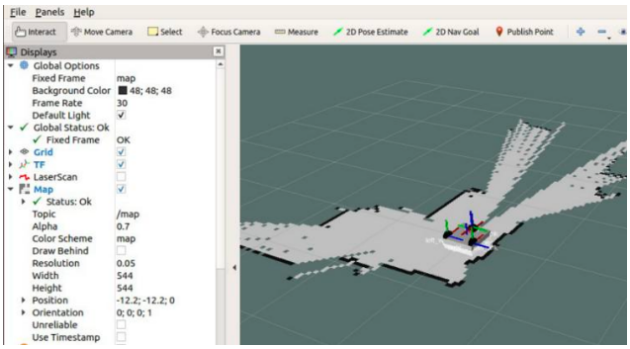

Figure 8: rviz visualization

2.3.4 Processor Subsystem

Our ROS-based controller utilizes the Raspberry Pi 4B, which features a quad-core ARM Cortex-A72 processor running at 1.5GHz and 4GB of RAM, delivering a computational performance of up to 0.2 TOPS. It is powered by a 5V supply. The Raspberry Pi runs the Robot Operating System (ROS) and manages communication with both the RGB camera and LiDAR sensor through their respective interfaces. The camera, connected via USB 2.0 and compliant with the UVC standard, streams RGB images to the Pi, where ROS-compatible computer vision algorithms are used for image processing. The STM32 microcontroller complements the Raspberry Pi by handling power distribution and control signaling. It features two integrated 5V power outputs—one dedicated to the STM32 and its peripherals (e.g., encoders, Bluetooth modules, and gamepads), and the other supplying power to the Raspberry Pi. In addition to power management, the STM32 also receives sensor data and executes control commands for the drive subsystem. This subsystem connects the sensor system to the drive system, ensuring the vehicle can automatically adjust its posture based on external information. Specifically, based on the source code of the F103VET6 mini vehicle, we use a Raspberry Pi 4B controller to receive information from the RGB camera and radar sensor, combining computer vision algorithms for further command processing and publishing. The STM32 microprocessor will receive and execute the commands.

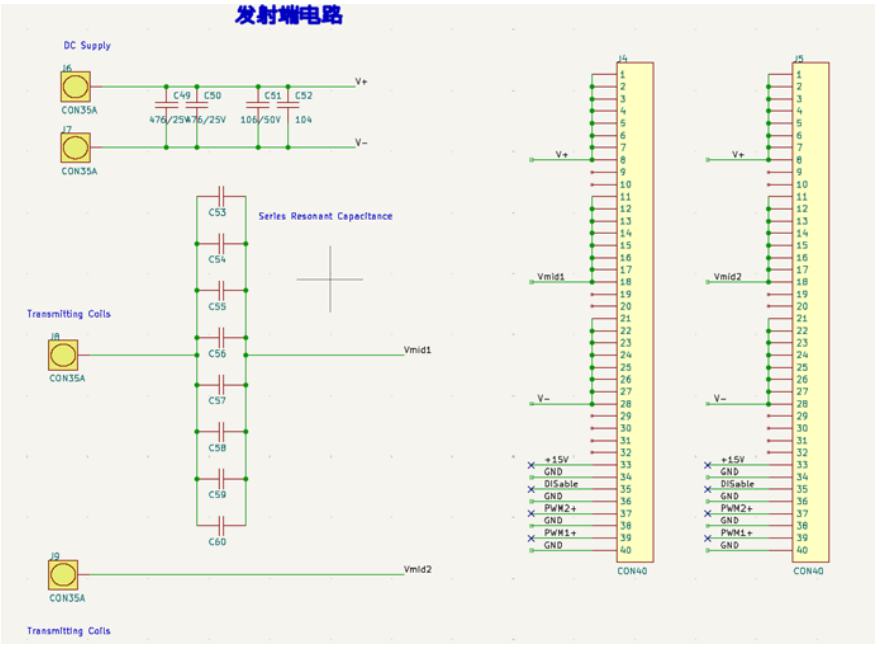

Figure 9: Transmitter PCB Board Schematic

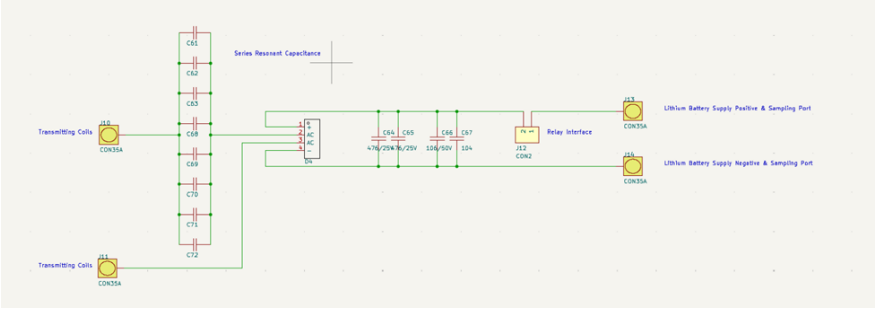

Figure 10: Reciever PCB Board Schematic

2.4 Subsystem Diagrams & Schematics

The PCB boards for the wireless charging system is shown in fig.9 and fig.10. They mainly contain compensating capacitor and two full bridges.

The chassis subsystem is shown in figure 11. It includes four Mecanum wheels, a metal frame, two acrylic shock absorber plates 1, two acrylic shock absorber plates 2, four base plates, eight hydraulic spring shock absorbers, two slide rails, and two sliders.

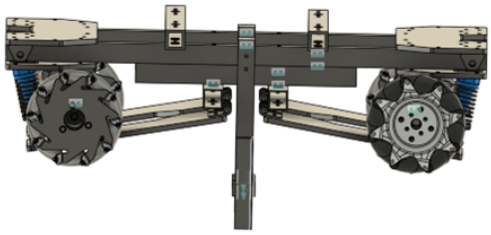

Figure 11: Chassis Subsystem

3 Cost&Schedule

3.1 Cost

Name	Description	Manufacturer	Qty	Total (yuan)
ADC	INA219 bidirectional current/voltage sensor module	TI	1	12.6
Micro-Controller	RaspberryPi 4B Microcontroller 8GB model with heat sink	Taobao	1	343.05
HDMI Cable	HDMI 2.0 compatible 4K 60Hz high-speed cable with Ethernet	UGREEN	1	29.9
SD Card Reader	USB 3.0 portable SD/TF card reader with multi-format support	UGREEN	1	28.8
STM32	STM32 microcontroller with embedded motor drive circuitry	WheelFun	1	299

Table 1: Component List with Automatic Text Wrapping

3.2 Schedule

Week	Task	Member
2.24	Specify Design Task and Requirements	Wei Yuyang, Jing Liheng
		Wang Yuhang
		Dong Hongye

Week	Task	Member
3.3	Install Ubuntu and ROS on a virtual machine	Wei Yuyang, Jing Liheng
	Literature Review; Circuit Analysis	Wang Yuhang
	Check the 3D model and determine the basic framework	Dong Hongye
3.10	Configure Ubuntu and ROS on a Raspberry Pi	Wei Yuyang, Jing Liheng
	Circuit Analysis	Wang Yuhang
	Communicate with team members and determine requirements	Dong Hongye
3.17	Set up Ubuntu and ROS on Jetson Nano	Wei Yuyang, Jing Liheng
	Matlab simulation and debugging	Wang Yuhang
	Detailed measurement of vehicle body and charging coil dimensions	Dong Hongye
3.24	Establish SSH wireless connection and NFS mount between the virtual machine and Raspberry Pi	Wei Yuyang, Jing Liheng

Week	**Task**	**Member**
	PCB board design	Wang Yuhang
	Modeling of other required components for the base	Dong Hongye
3.31	Lidar mapping and autonomous navigation	Wei Yuyang, Jing Liheng
	Wiring of two microcontrollers	Wang Yuhang
	3D printing based on the model and installing it on the car	Dong Hongye
4.7	Writing Design Document	Wei Yuyang, Jing Liheng
	Testing of charging coils	Wang Yuhang
	Test the practicality of the parts	Dong Hongye
4.14	Integrate the ADC module and establish real-time power monitoring	Wei Yuyang, Jing Liheng
	Build the test environment for PCB boards	Wang Yuhang
	Test and debug PCB boards	Dong Hongye
4.21	Develop and test the positioning algorithm to maximize charging efficiency	Wei Yuyang, Jing Liheng
	Test and debug PCB boards	Wang Yuhang

Week	**Task**	**Member**
	Test the practicality of the parts and make improvements	Dong Hongye
4.28	Laborer Holiday	Wei Yuyang, Jing Liheng
		Wang Yuhang
		Dong Hongye
5.5	Refine autonomous navigation for dynamic environments	Wei Yuyang, Jing Liheng
	Retest the charging coils and prepare for systematic testing	Wang Yuhang
	Finish product tests and iterations	Dong Hongye
5.12	Systematic testing	Wei Yuyang, Jing Liheng
	Finish product tests and iterations	Wang Yuhang
		Dong Hongye

Table 2: Task Schedule and Member Assignments

4 Requirements&Verification

4.1 Completeness of Requirements

In general, all high-level requirements are accomplished or within tolerable deviation. A 12V battery is used as the energy storage. The car can move at a maximum speed of 1 m/s. The wireless charging can give the battery's rated charging voltage. The car can align to the charging coil within 7 minutes automatically. The place of the charging station is recognized by a special obstacle on the map. Three boxes are avoided during the navigation process.

4.2 Appropriate Verification Procedures

The speed of the car is measured by setting a distance of 2m and using a stopwatch The battery is present with its parameters printed on the box.

The procedure of verifying wireless charging system is conducted through input setting and output measuring.The input voltage is set to 34V DC. The control signal is square wave function with amplitude Vpp = 4V and frequency at 85kHz. The output signal is measured by an Oscilliscope connected to the output portal of receiver. The output portals should also be connected to the battery's terminals. The criterion for success is that the output voltage is equal to or greater than 12.6 V.[3] As shown in figure.12, our output of the charging system is a constant voltage output with proper voltage regulation.

SB 2.0 bandwidth tests stress the camera subsystem with continuous RGB/depth frame transfers for one hour, checking for packet loss, jitter, and physical weaknesses via cable strain. LiDAR UART communication is validated during rapid maneuvers to ensure error-free data. Reflective targets measure SLAM's absolute positioning accuracy, while extended navigation trials assess localization consistency and odometry drift, guiding algorithmic refinements. These tests validate hardware durability, communication reliability, and system precision.

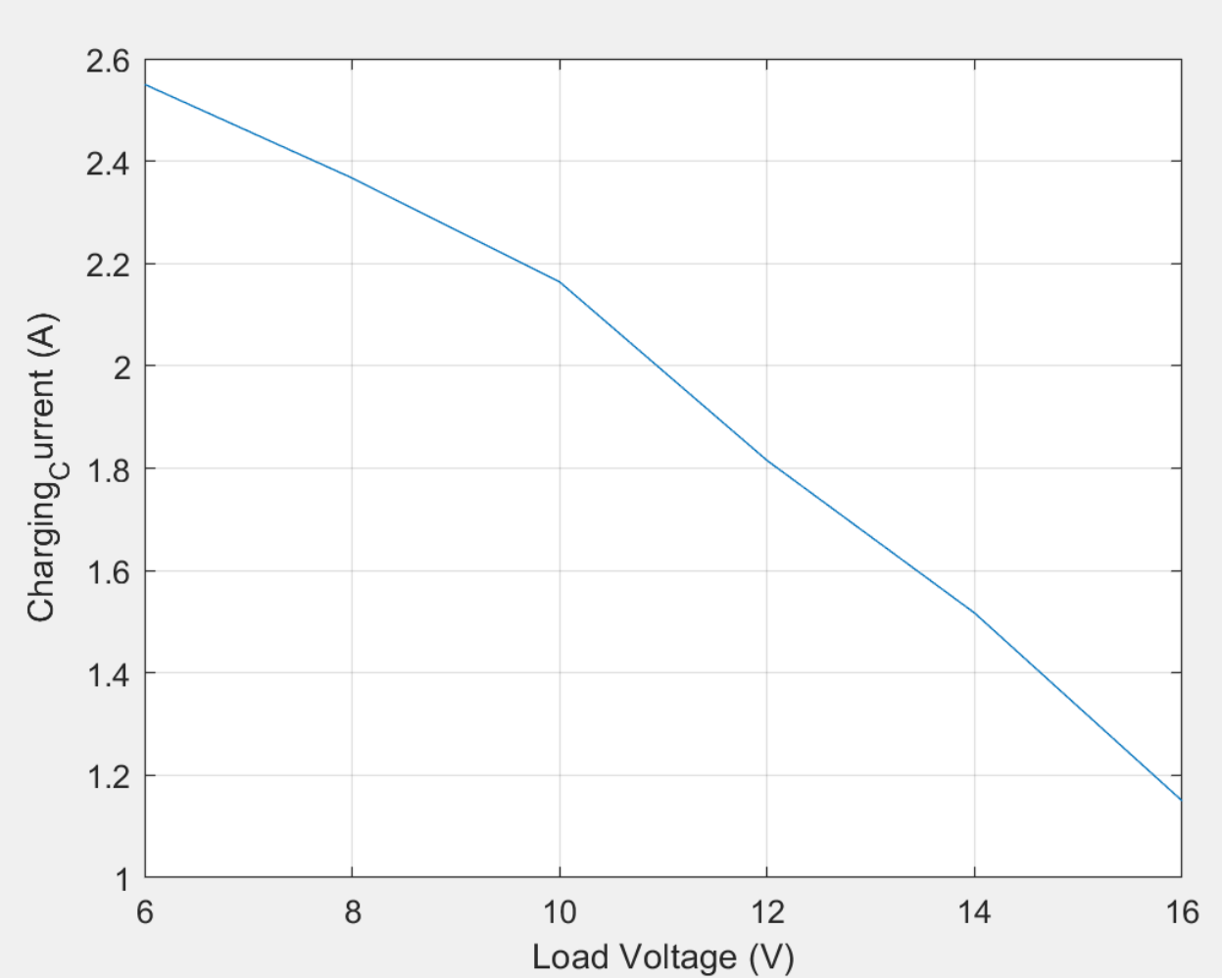

Figure 12: Verification Plot

For the base subsystem, our requirement is to be able to maintain the cart chassis level on uneven terrain to improve wireless charging efficiency. And stabilize the overall posture of the cart to ensure consistent performance and accuracy in camera recognition. To verify the above two requirements, we placed the shock absorption structure of the trolley on a test surface with flat ground on the left and a 10 ° slope on the right. The wireless charging efficiency remained above 85% and the camera maintained normal recognition of obstacles.

4.3 Quantitative Results

The speed of the car is at 1 m/s. The wireless charging voltage for battery is equal to or greater than 12.6 V. The overall charging efficiency is at 60% as shown in the following table.

Raspberry Pi 4 Model B Operating temperature: 0-50 Input power: 5V DC via USB-C connector (minimum 3A), 5V DC via GPIO header (minimum 3A), Power over Ethernet (POE) – enabled Connectivity: 2.4 GHz and 5.0 GHz IEEE 802.11b/g/n/ac wireless LAN, Bluetooth 5.0, BLE Processor: Broadcom BCM2711, quad-core Cortex-A72 (ARM v8) 64-bit Soc @ 1.5GHz

STM32 Core: Arm® 32-bit Cortex®-M4 CPU with FPU, Adaptive real-time accelerator (ART Accelerator) allowing 0-wait state execution from flash memory, frequency up to 168 MHz, memory protection unit, 210 DMIPS/ 1.25 DMIPS/MHz (Dhrystone 2.1), and DSP instructions Memories – Up to 1 Mbyte of flash memory – Up to 192+4 Kbytes of SRAM including 64- Kbyte of CCM (core coupled memory) data RAM – 512 bytes of OTP memory – Flexible static memory controller supporting Compact Flash, SRAM, PSRAM, NOR and NAND memories 3×12-bit, 2.4 MSPS A/D converters: up to 24 channels and 7.2 MSPS in triple interleaved mode 2×12-bit D/A converters Up to 17 timers: up to twelve 16-bit and two 32- bit timers up to 168 MHz, each with up to 4 IC/OC/PWM or pulse counter and quadrature (incremental) encoder input Up to 3 × I2C interfaces (SMBus/PMBus)

Input	Output	Efficiency
21V/0.557A/11.7W	12.47V/0.547A/6.816W	58.26%

Raspberry Pi 4 Model B

Operating temperature: 0-50. Input power: 5V DC via USB-C connector (minimum 3A), 5V DC via GPIO header (minimum 3A), Power over Ethernet (POE) – enabled. Connectivity: 2.4 GHz and 5.0 GHz IEEE 802.11b/g/n/ac wireless LAN, Bluetooth 5.0, BLE. Processor: Broadcom BCM2711, quad-core Cortex-A72 (ARM v8) 64-bit Soc @ 1.5GHz

STM32

Core: Arm® 32-bit Cortex®-M4 CPU with FPU, Adaptive real-time accelerator (ART Accelerator) allowing 0-wait state execution from flash memory, frequency up to 168 MHz, memory protection unit, 210 DMIPS/ 1.25 DMIPS/MHz (Dhrystone 2.1), and DSP instructions

Memories – Up to 1 Mbyte of flash memory – Up to 192+4 Kbytes of SRAM including 64-Kbyte of CCM (core coupled memory) data RAM – 512 bytes of OTP memory – Flexible static memory controller supporting Compact Flash, SRAM, PSRAM, NOR and NAND memories The vehicle was fabricated according to design specifications, with critical dimensions verified using precision measuring instruments. The results are presented in the following table. Also, the total mass of the vehicle is 5kg.

Parameter	Design Value (mm)	Measured Value (mm)
Overall length	320	318
Overall width	180	182
Overall height	200	198
Wheel diameter	64	64.5

5 Conclusion

5.1 Accomplishments

The project successfully demonstrates a self-navigating vehicle powered by a 12V battery, capable of autonomously traversing dynamic environments while integrating seamless wireless charging. Central to its functionality is a real-time mapping algorithm embedded within a Raspberry Pi microcontroller, which constructs and visualizes a 3D model of the physical environment using sensor data, enabling the vehicle to adapt to obstacles and complex layouts such as mazes. Though tested with three strategically placed obstacles, the system's scalable design allows it to handle far more intricate scenarios, leveraging continuous environmental updates to optimize path planning. Complementing this navigation prowess is a robust wireless charging system, rigorously validated in lab conditions to safely endure high-power demands of 10A current and 50V voltage. Critical to its reliability is the precision-engineered mechanical design, featuring an alignment-focused hanger and base that ensure consistent charging connectivity even during positional variances. Together, these innovations culminate in a fully autonomous platform that merges adaptive intelligence, resilient power management, and hardware precision.

5.2 Uncertainties

The alignment algorithm is handicapped by poor control over the motors. As we are using DC motors, advanced control strategies are needed. Compared to step motors, DC motors used in this project is greatly affected by battery voltage, small bumps on the base, and some physical parasitic randomness of movements. Even if we have provided the same speed setting for the same amount of time, the displacement varies greatly.

The charging system designed has room for improvements in the sense that the coupling between coils is small. Due to the compactness of the charging system, larger or thicker coils are unavailable.

5.3 Future Work / Alternatives

Future optimizations of the design can be divided into three parts: programming upgrade, electrical upgrade, and mechanical upgrade.

- programming upgrade.
  Although the performance of our designed hill-climbing algorithm is satisfied, the robustness of the algorithm still has room for improvement. In the future, we could take the interaction with the physical environment into account. For now, we assume the car is moving in a flat ground. However, the charging station could be placed on complex environment situation outside of the lab. We could take some of the existing advanced algorithm as reference and make our algorithm as robust as possible to work in any complicated situation.

- electrical upgrade
  The wireless charging system currently has an efficiency of 66%. In addition to improvements from other subsystems, the charging coils and PCB boards are also available for optimization. Connections between elements such as PCB boards and coils are mostly tape or screws. This type of connection prototype can be soldered or integrated to improve efficiency due to lower unwanted resistance. Turns of reciever coil can be enlarged if we use two or more layers of windings. Multiple layers of windings may cause other problems that needs to be studied.

5.4 Ethical Considerations

1. Safety Accountability

Our autonomous charging vehicle employs a multi-layered safety system featuring high-precision LiDAR and radar sensors for comprehensive environmental detection. The system incorporates real-time emergency braking that activates within milliseconds when obstacles are detected, ensuring reliable collision avoidance in dynamic environments. Furthermore, all safety-critical components are designed with redundancy and undergo rigorous testing to meet international safety standards.

2. Privacy Protection

The vehicle's mapping and navigation system processes all spatial data exclusively on-device, eliminating any cloud storage or transmission of sensitive environmental information. We've implemented end-to-end encryption for any temporarily stored operational data, with automatic purging cycles to prevent long-term data retention. Users maintain full control through a transparent data management interface that allows complete deletion of all stored maps and navigation history at any time.

3. Energy Environmental Ethics

Our dynamic charging algorithm continuously monitors power requirements and grid conditions to optimize energy usage, reducing standby consumption by up to 40 percent compared to conventional systems. The modular battery design features quick-release mechanisms and standardized cells to facilitate repairs and recycling. We've partnered with certified e-waste processors to ensure responsible end-of-life battery disposal, while using larger than 30 percent recycled materials in new battery production to support circular economy principles.

References

[1] X. Wu, H. Xu, J. Xiao, Y. Mo, N. Wu, and S. Chen, "Overview of wireless power supply technology for electric vehicles," in *2023 IEEE 6th International Conference on Automation, Electronics and Electrical Engineering (AUTEEE)*, IEEE, Dec. 2023, pp. 66–69. DOI: 10.1109/AUTEEE60196.2023.10408533.

[2] W. C. Brown, "The history of power transmission by radio waves," *IEEE Transactions on Microwave Theory and Techniques*, vol. 32, no. 9, pp. 1230–1242, Sep. 1984. DOI: 10.1109/TMTT.1984.1132833.

[3] X. Li and A. K. S. Bhat, "Analysis and design of high-frequency isolated dual-bridge series resonant DC/DC converter," *IEEE Transactions on Power Electronics*, vol. 25, no. 4, pp. 850–862, Apr. 2010. DOI: 10.1109/TPEL.2009.2034662.